Lecture 3 SCATTERER INVERSION
Subject 1 Seismic Path and Site Effect Estimation based upon Scatterer Inversion

1. INTRODUCTION

At present, we have a variety of tools for strong motion synthesis. In other words, we can perform the forward modeling type of problems considerably well. Also, the techniques to infer independent parameters have been constructed with some confidence in the long-period range of more than several seconds. However, the reliable estimation of independent parameters corresponding to high-frequency components of motion remains unsolved. This sort of problem should be solved using inversion technique. The inversion problem requires both formulation for the forward modeling and inversion technique to determine independent parameters as uniquely and exactly as we can Although the inversion technique is very powerful, it is essentially accompanied by some mathematical difficulties.

Iida has concentrated on the estimation of high-frequency strong ground motion in the near-source regions, which is probably the most important subject of earthquake disaster prevention. Deterministic approaches are used. The reasons why he employs deterministic approaches are: they are more directly applicable to prediction problems. and the results may be verified using other information.

2. HIGH-FREQUENCY SOURCE INVERSION

Undoubtedly, source effects are primarily important in the near-source regions. To estimate source effects in the high-frequency range, near-source records are adequate because the path effects are relatively minor. It is also recommended to choose a data set which is not much influenced by local site effects. But we have very few such array seismograms from large earthquakes.

A suitable method to estimate source effects in the high-frequency range seems to treat a system of elastodynamic linear equations relating the unknown fault slip distribution vectors with the recorded ground motion data vectors through a matrix of the Green's functions for the medium, with reasonable and physical constraints, as Olson and Apsel (1982) or Hartzell and Heaton (1983) performed. In this method with actual velocity models, the fault rupture process can be analyzed in detail, giving realistic results. Nevertheless, source effects that are closely related to damage and intensity patterns have not been confirmed. The most likely reason is lack of well-instrumented earthquakes.

Hartzell and Iida (1990) applied a modified version of the Hartzell and Heaton's method to the 1987 Whittier Narrows, California earthquake, which is one of the best instrumented earthquakes to date. Leyendecker *et al.* (1988) noted the unusual damage and intensity patterns of this earthquake [Fig 1]. The pattern of 17 near-source stations that forms good azimuthal coverage of the source is expected to give good resolution (Iida, 1990). Band-pass filtered velocity records from 0.2 to 3.0 Hz were used. This frequency range is responsible for much of an earthquake's damage and intensity. The Green's function for a velocity gradient model included all theoretical arrivals. No local effects were taken into account.

3. IMPLICATIONS OF HIGH-FREQUENCY INVERSION

---

* This lecture note is based on the paper of the same title written by Masahiro Iida and Paul Spudich, published on "Proc. 2nd SEGJ/SEG (Soc. Exploration Geophysicists Japan / Soc. Explo. Geophys.) Int. Symp. Geotomography, pp. 57-76, Tokyo, Japan, November 1992".

The slip distributions for 3 rupture models commonly indicated a complex rupture process within a small source volume [Fig. 2]. The data records were compared with the synthetics for the latter 2 rupture models in Fig. 3. The waveforms are fit well in both shape and amplitude, especially for the earlier parts of the records. The same tendency had been recognized in previous inversion studies (Olson and Apsel, 1982; Hartzell and Heaton, 1983). We should note that the large-amplitude sections are not influenced by local site effects. The later parts of the records most likely contain propagation path effects not included in our simple model.

In order to interpret the unusual damage and intensity patterns, the peak velocities in the epicentral region were predicted on the basis of the inferred distribution of slip. The result for the model (b) of Fig. 2 is shown in Fig. 1, where peak velocities are contoured. It is consistent with intensity and damage distributions. This result demonstrated source effects in the high-frequency range, which had not been confirmed by interference with severe local site effects and by insufficient station distribution to conduct source inversion.

4. SPATIAL RESOLUTION AND STATION-ARRAY LAYOUT FOR SOURCE INVERSION

Large inconsistencies have been often seen among source inversion results. Such typical inconsistency was exemplified in the 1979 Imperial Valley earthquake (e.g., Olson and Apsel, 1982; Hartzell and Heaton, 1983; Archuleta, 1984). The inconsistencies seem to come mainly from the insufficient station distribution.

At the International Workshop on Strong-Motion Earthquake Instrumented Arrays held in 1978 (Iwan, 1978), a preferable array configuration was first proposed on the basis of empirical judgement. Subsequently, only few quantitative attempts (Spudich and Oppenheimer, 1986; Miyatake *et al* , 1986) were started to estimate effects of station array. Although the early studies used too simple Green's functions, the significance of good strong-motion array was shown.

Therefore, we need to estimate the possible spatial resolution obtained by a specific array network in order to understand limitations of current source inversion studies and to provide the installation plan of strong-motion station arrays for source studies.

Iida *et al.* (1990b) developed an overdetermined least-squares inversion scheme, where the spatial resolution was predetermined by the subfault size and the model variance was used as the accuracy of the source inversion. The accuracy of source inversion was efficiently estimated by using Wolberg's prediction analysis. A complete Green's function in a semi-infinite elastic space was used. On the basis of this scheme, a systematic analysis was done to obtain relationship between the accuracy of the source inversion (the solution variance) and fault-array parameters (Iida *et al.*, 1990b). This simulation tells us that, while just an increase in the number of stations is not effective, the azimuthal coverage of the source and the array size should be considered. The estimated optimum array configuration for source inversion in each of 3 typical faults (Iida, 1990) [Fig. 4] was consistent with the one proposed at the International Workshop (Iwan, 1978). It implies that the goodness of array configuration can be quantitatively measured by this method. The resolving power of existing array networks was evaluated, providing us with the possible spatial resolution by each array (Iida *et al* , 1990a)

5. STRONG-MOTION ARRAY DESIGN AND IDEAL SOURCE INVERSION

Invoking physical (seismic) wave simulations (Iida *et al.*, 1990b), design policy of strong-motion array layout was provided (Iida, 1992). If we consider an intermediate frequency band (several seconds to several Hz), the above studies are effective. We should choose an inversion method of solving normal equations or an iterative least-squares inversion method (Kikuchi and Kanamori, 1982), using complete Green's function First, according to the fault mechanism, a desirable array configuration is determined. Secondly, assuming the spatial resolution and the inversion accuracy required, the number of array stations is determined. If the target frequency is very high (more than several Hz), a differential-array inversion analysis (Spudich and Cranswick, 1984) is recommended using only

body waves. In this case, an array design proposed by Spudich and Oppenheimer (1986) is available

Finally, ideal source inversion in the high-frequency range is briefly summarized [Fig. 5]. The reliability of source inversion is reasonably measured by 'Spatial resolution', 'Waveform matching' and 'Intensity pattern matching'. More importantly, the limitations of source inversion depend on the quality and quantity of the available data set, and they can be estimated based upon 'Array layout' and 'Physical waves'.

6. PATH AND SITE EFFECTS

On the other hand, path and site effect cannot be ignored in most cases because we come to recognize that source effect, path effect and site effect jointly affect strong-motion seismograms. This was symbolically shown by the 1985 Michoacan, Mexico earthquake (e.g., Campillo *et al.*, 1989). It has been verified by numerous studies that high-frequency strong motion is heavily affected by local site effect including soil nonlinear behavior. This situation was summarized by Aki (1988) The formulation of path effect is considered to be more difficult than the formulation of source and site effect, because path effect is very complicated due to some heterogeneity in underground structure. In near-source regions, however, path effect becomes comparatively simple since only body waves are important in most cases. In Fig. 3, we could explain early phases, but it was impossible to interpret the late phases. The late phases are perhaps produced in the propagation path. Although we move to path effect, our methods are based upon source formulation, and the evaluation of local site effect is simultaneously done.

7. LOCAL HETEROGENEITIES, SCATTERING AND CODA

Body waves are dominant in near-source seismograms. Important factors for body wave propagation are attenuation and scattering (a phenomenon that a ray is reflected by a local heterogeneity). Both factors are related to local heterogeneities. Although we have a certain formulation for attenuation, evaluation of scattering effects is not so simple. We restrict ourselves to scattering.

There are 2 types of approaches for scattering. The statistical approach is based upon the concept that coda parts (later phases after S wave arrivals) [Fig. 6] have common characteristics owing to the similarity in propagating paths because coda parts comprise many rays which have experienced different paths. In contrast, the deterministic approach comes from the idea that coda parts have some distinct differences, giving characteristic information on the ray paths

In general, it has been considered that local heterogeneities can no longer be inferred in a deterministic way mainly due to the large number of parameters required and the data quality. Some of scattering problems began to be solved when some seismologists started using statistical approaches, bypassing deterministic approaches, in the late 1960's and early 1970's. Its application to high-frequency records was pioneered by Aki (1969). The requirement of a more realistic model has been clearly shown, and more recent studies move in this direction.

8. PURPOSE

We (Spudich and Iida, 1992) are developing a waveform scatterer inversion, which is a deterministic approach. Our twofold purposes are to locate the local heterogeneities that are responsible for scattering energy to the site of interest, and to characterize the seismic response of these heterogeneities. We deal with early S wave coda parts. From an engineering standpoint, the seismic coda changes the amplitude level of large-amplitude sections and increases the duration of strong shaking, causing progressive damage to buildings, as was observed in Mexico City during the 1985 Michoacan earthquake.

We use microearthquake seismograms. Microearthquakes can be treated as point sources and such seismograms are easy to obtain. For the last decade, strong-motion seismograms from large earthquakes have been

synthesized based upon a summation method of seismograms from small earthquakes (empirical Green's functions) (e.g., Hartzell, 1978; Iida and Hakuno, 1984). Then, path effects are automatically incorporated into the method, and we do not need any calculations to evaluate Green's functions. Our present method might be another good use of the records from small earthquakes.

9. DETERMINISTIC INTERPRETATION OF SCATTERED WAVE FIELD

Only a limited number of studies on deterministic interpretation of scattered wave field have been attempted, but recently an increasing number of researchers are engaged in this study scope. A first attempt was the analysis of the Eskdalemuir array data by Key (1967) in which an azimuth and velocity search through the coda revealed the presence of a strong isolated arrival produced by P to Layleigh wave conversion at a particular location. This sort of research in deterministic interpretation and modeling of P coda at teleseismic distances was subsequently carried on by Nikolaev and Troitskiy (1987), Lay (1987), and most recently Hedlin *et al.* (1991). Lay, using a source array, and Nikolaev and Troitskiy, who used a receiver array, assumed that a Green's function describing propagation from the source to the scattering point was a teleseismic P body wave, but assumed nothing about scattered waves. These assumptions led them to a stacking procedure to determine scatterer strength, and they used the semblance of the stack and isotropic scatterers. Hedlin *et al.* attempted to map near-source and near-receiver scatterer distribution. On the other hand, the coda of local earthquakes has been very extensively studied, as summarized by Herraiz and Espinoza (1987). An interesting study by the deterministic way was done by Nishigami (1991), who determined a spatial scatterer distribution by using a technique similar to those used for teleseismic P coda.

Our current study is based upon Spudich and Miller's study (1990). They concentrated upon source mechanisms, P- and S-wave travel-time variations, and variations in the site transfer function in order to characterize microearthquake sources to have different seismograms at a common site. The site transfer function was expressed as a sum of several terms having simple dependences upon the incidence angle and the azimuth. Each term was an independent function of time. Their problem may be regarded as a spatial interpolation of seismograms. The interpolation technique was not very successful in providing accurate seismograms for sources located outside the aftershock volume. The primary cause was the likely scattering of seismic waves by local heterogeneities.

10. METHODS

Our methods are a modified version of the computational method of Spudich and Miller (1990). The general procedure consists of 2 steps. First, we identify the geological heterogeneities in the study region which contribute substantial scattered energy to the observed seismic coda. Secondly, having identified these heterogeneities, we determine their time-domain contributions to the observed codas.

In our approach, we use a set of seismograms from widely distributed local earthquakes observed at a single station. The analyses are done independently for each component of motion. In the reciprocal geometry, a point force is applied at the station. It radiates some waves, and they are incident upon hypothetical scatterers at ξ_1, ξ_2, .., etc. The incident waves make the scatterers radiate like equivalent 3 body forces and 6 moment tensor secondary sources having complicated time-functions, $Fi(\xi,t)$ and $Mjk(\xi,t)$. The radiation from the scatterers propagates to an earthquake, q_1 [Fig. 7]. We use the observed waveform seismograms to solve for the average $Fi(\xi,t)$ and $Mjk(\xi,t)$ at each scatterer. Thus, the scattering problem can be turned into a radiation problem, forming an inverse problem. For example, Wu and Aki (1985) represented the scattered field by a radiation field of equivalent sources

Our general model is that the top few km of the earth are much more heterogeneous than the deeper part, so that it is impossible to model wave propagation accurately in the shallow crust at high frequencies. Consequently our method assumes nothing about the Green's functions in the shallow crust, while it assumes that geometric ray theory is adequate below a few km depth. A key concept is that the complicated wave field produced by scattering

in a heterogeneous structure can be simulated by complicated artificial sources acting in a simple structure.

This set of assumptions leads to a linear system for the force and moment tensor time series for each hypothetical scatterer. The solution is obtained by using an iterative tomographic method (Olson, 1987). From these approximate force and moment time series, the predicted seismogram for each earthquake is calculated. For display purposes, we reduce all the time series for a scatterer down to a single scalar representing the intensity We define the power in the force vector time series $F_i(\xi,t)$ as

$$P_{Fi}(\xi) = \frac{1}{T}\int_0^T \{\dot{F}_i(\xi,t)\}^2 dt$$

With a similar definition for the power in the moment tensor, we define the average power $P(\xi)$ to be

$$P(\xi) = P_{F1}(\xi) + P_{F2}(\xi) + \cdots + P_{M33}(\xi)$$

Here powers in the force and moment terms have the same units by introducing a weighing.

11. APPLICATION TO NORTH PALM SPRINGS AFTERSHOCKS

We apply this technique to aftershock recordings made at 3 strong motion stations, SMP, SMC and SUB that recorded the 1986 North Palm Springs, California earthquake [Fig. 8]. As our first step, we perform surface scatterer inversion because it is expected that most scatterers are concentrated near the ground surface. We set a grid of 16 x 16 scatterers having a 2 km separation in each dimension. The approximate bandwidth of the data used is 2-4 Hz, and we show power distributions in a 13.0 sec window following the direct S wave

The power distribution for the N-S component of SMP early coda is quite similar to that for the E-W component [Fig. 9]. We can see that the coda power peak 8 km west of SMP falls at the contact of the alluvium with the older Pleistocene sedimentary deposits. For brevity we call this particular point as point F [Fig. 8]. The power peak at F represents waves that travel as S waves from the aftershock hypocenters to the edge of the alluvium and then travel to SMP.

The big surprise comes when we examine the coda power distribution at station SMC, located in the Morongo Valley, which is completely separate form the Coachella Valley. Point F appears to scatter strongly into the coda at SMC [Fig 10] Thus, point F can be identified in data from 2 separate stations and is almost certainly real.

In contrast, it is surprising that waves scattered from point F are not observed at station SUB inside the valley. The power distributions for SUB are indistinct [Fig. 11] perhaps because most coda power is scattered from the western edge of the valley.

In summary, on all stations and components except SUB-EW, we observe a power peak at or near the station that may represent energy reverberating very near the station. For both components of SMC and SMP, we observe a power peak located at point F at the northwest end of the alluvium in the Coachella Valley. On both components of SUB we fail to observe a peak at F, but rather see a peak a few km west of SUB.

12. THE NATURE OF THE SCATTERED WAVES

We conduct the following tests which demonstrate that laterally scattered S body waves are an important component

at least at SMP. We have run the inversion of the SMP-NS coda data again, but this time we use only 2 scatterers, one at the station SMP and one at F. Fig. 12 shows that part of energy scattered from F to SMP is a S body wave. The diamonds mark a conspicuous phase that follows S. The squares mark the initiation of the ground motions caused by scattering from F. Point F contributes a burst of energy that agrees quite well in arrival time with the observed later phase.

The scattered waves continue for several seconds. They might be body waves or surface waves. The former case includes both possibilities of upgoing body waves and S waves diffracted from the basin edge and refracted along the top of the basement. When we see ample theoretical evidence for nonuniform scattering from basin edges (e g., Hill *et al.*, 1990; Horike *et al.*, 1990), almost all of this evidence concerns scattering of surface waves into the basin.

13. CONCLUDING REMARKS

(1) Impedance contrasts at the edges of valleys may scatter waves more strongly than do topographic features.

(2) We have identified horizontally propagating waves at all 3 sites studied, both inside and outside the Coachella Valley. This suggests that simple 1-D models of soil column response are inadequate in some cases.

(3) Particular places at the edges of alluvial valleys appear to be 'bright spots,' i.e., loci of particularly strong scattering. These bright spots can be identified by both source and receiver array studies of microearthquakes.

14. REFERENCES

Aki, K. (1969). Analysis of the seismic coda of local earthquakes as scattered waves, *J. Geophys. Res.*, **74**, 615-631.

Aki, K. (1988). Local site effects on strong ground motion, *Proc. Earthq. Eng. Soil Dynamics II -- Recent advances in ground motion evaluation*, 103-155, Park City, Utah, USA.

Archuleta, R.J. (1984). A faulting model for the 1979 Imperial Valley earthquake, *J. Geophys. Res.*, **89**, 4559-4585.

Campillo, M., J.C. Gariel, K. Aki and F.J. Sanchez-Sesma (1989). Destructive strong ground motion in Mexico City· Source, path and site effects during the 1985 Michoacan earthquake, *Bull. Seism. Soc. Am.*, **79**, 1718-1735.

Hartzell, S.H. (1978). Earthquake aftershocks as Green's functions, *Geophys. Res. Lett.*, **5**, 1-4.

Hartzell, S.H. and T.H. Heaton (1983). Inversion of strong motion and teleseismic waveform for the fault rupture history of the 1979 Imperial Valley, California, earthquake, *Bull. Seism. Soc. Am.*, **73**, 1553-1583.

Hartzell, S and M. Iida (1990). Source complexity of the 1987 Whittier Narrows, California, earthquake from the inversion of strong motion records, *J. Geophys. Res.*, **95B**, 12475-12485.

Hedlin, M A.H., J.B. Minster and J.A. Orcutt (1991). Beam stack imaging using a small aperture array, *Geophys. Res. Lett.*, **18**, 1771-1774.

Herraiz, M and A.F. Espinoza (1987). Coda waves: a review, *Pure Appl. Geophys.*, **125**, 499-577.

Hill, J., H. Benz, M. Murphy and G. Schuster (1990). Propagation and resonance of SH waves in the Salt

Lake Valley, Utah, *Bull. Seism. Soc. Am.*, **80**, 23-42.

Horike, M., H. Uebayashi and Y. Takeuchi (1990). Seismic response in three-dimensional sedimentary basin due to plane S wave incidence, *J. Phys. Earth*, **38**, 261-284.

Iida, M. (1990). Optimum strong-motion array geometry for source inversion -- II, *Earthq. Eng. Struct. Dyn.*, **19**, 35-44.

Iida, M. (1992). Source effects on strong-motion records and resolving power of strong-motion arrays for source inversion, *Tectonophysics* (in print).

Iida, M. and M. Hakuno (1984). The differences in the complexities between the 1978 Miyagiken-oki earthquake and the 1968 Tokachi-oki earthquake from a viewpoint of the short-period range, *Natural Disaster Science*, **6**, 1-26.

Iida, M., T. Miyatake and K. Shimazaki (1990a). Preliminary analysis of resolving power of existing strong-motion arrays for source inversion, *J. Phys. Earth*, **38**, 285-304.

Iida, M., T. Miyatake and K. Shimazaki (1990b). Relationship between strong-motion array parameters and the accuracy of source inversion, *Bull. Seism. Soc. Am.*, **80**, 1533-1552.

Iwan, W.D. (Editor) (1978). Strong-motion earthquake instrument array, *Proc. Int. Workshop Strong-Motion Earthquake Instrument Arrays*, Honolulu, Hawaii, USA.

Key, F.A. (1967). Signal-generated noise recorded at the Eskdalemuir seismometer array station, *Bull. Seism. Soc. Am.*, **57**, 27-37.

Kikuchi, M. and H. Kanamori (1982). Inversion of complex body waves, *Bull. Seism. Soc. Am.*, **72**, 491-506.

Lay, T. (1987). Analysis of near-source contributions to early P-wave coda for underground explosions. III. Inversion for isotropic scatterers, *Bull. Seism. Soc. Am.*, **77**, 1767-1783.

Leyendecker, E.V., L.M. Highland, M. Hopper, E.P. Arnold, P. Thenhaus and P. Powers (1988). The Whittier Narrows, California earthquake of October 1, 1987 -- Early results of isoseismal studies and damage surveys, *Earthquake Spectra*, **4**, 1-10.

Miyatake, T., M. Iida and K. Shimazaki (1986). The effect of strong-motion array configuration on source inversion, *Bull. Seism. Soc. Am.*, **72**, 491-506.

Nikolaev, A.V. and P.A. Troitskiy (1987). Lithospheric studies based on array analysis of P-coda and microseisms, *Tectonophysics*, **140**, 103-113.

Nishigami, K. (1991). A new inversion method of coda waveforms to determine spatial distribution of coda scatterers in the crust and uppermost mantle, *Geophys. Res. Lett.*, **18**, 2225-2228.

Olson, A.H. (1987) A Chebyshchev condition for accelerating convergence of iterative tomographic methods: solving large least squares problems, *Phys. Earth Planet Interiors*, **47**, 333-345

Olson, A.H. and R.J. Apsel (1982). Finite faults and inverse theory with applications to the 1979 Imperial Valley earthquake, *Bull. Seism. Soc. Am.*, **72**, 1969-2001.

Spudich, P. and E. Cranswick (1984). Direct observation of rupture propagation during the 1979 Imperial

Valley earthquake using a short baseline accelerometer array, *Bull. Seism. Soc. Am.*, **74**, 2083-2114.

Spudich, P. and M Iida (1992). The seismic coda, site effects and scattering in alluvial basins studied using aftershocks of the 1986 North Palm Springs, California, earthquake as source arrays, *Bull Seism. Soc. Am.* (submitted).

Spudich, P. and D.P. Miller (1990). Seismic site effects and the spatial interpolation of earthquake seismograms: Results using aftershocks of the 1986 North Palm Springs, California, earthquake, *Bull. Seism. Soc. Am.*, **80**, 1504-1532.

Spudich, P. and D. Oppenheimer (1986). Dense seismograph array observations of earthquake rupture dynamics, in S. Das (Editor), *Earthquake Source Mechanics, Geophys. Monograph*, **37**, 285-296.

Wu, R.S. and K. Aki (1985). Scattering characteristics of elastic waves by an elastic heterogeneity, *Geophysics*, **50**, 582-595.

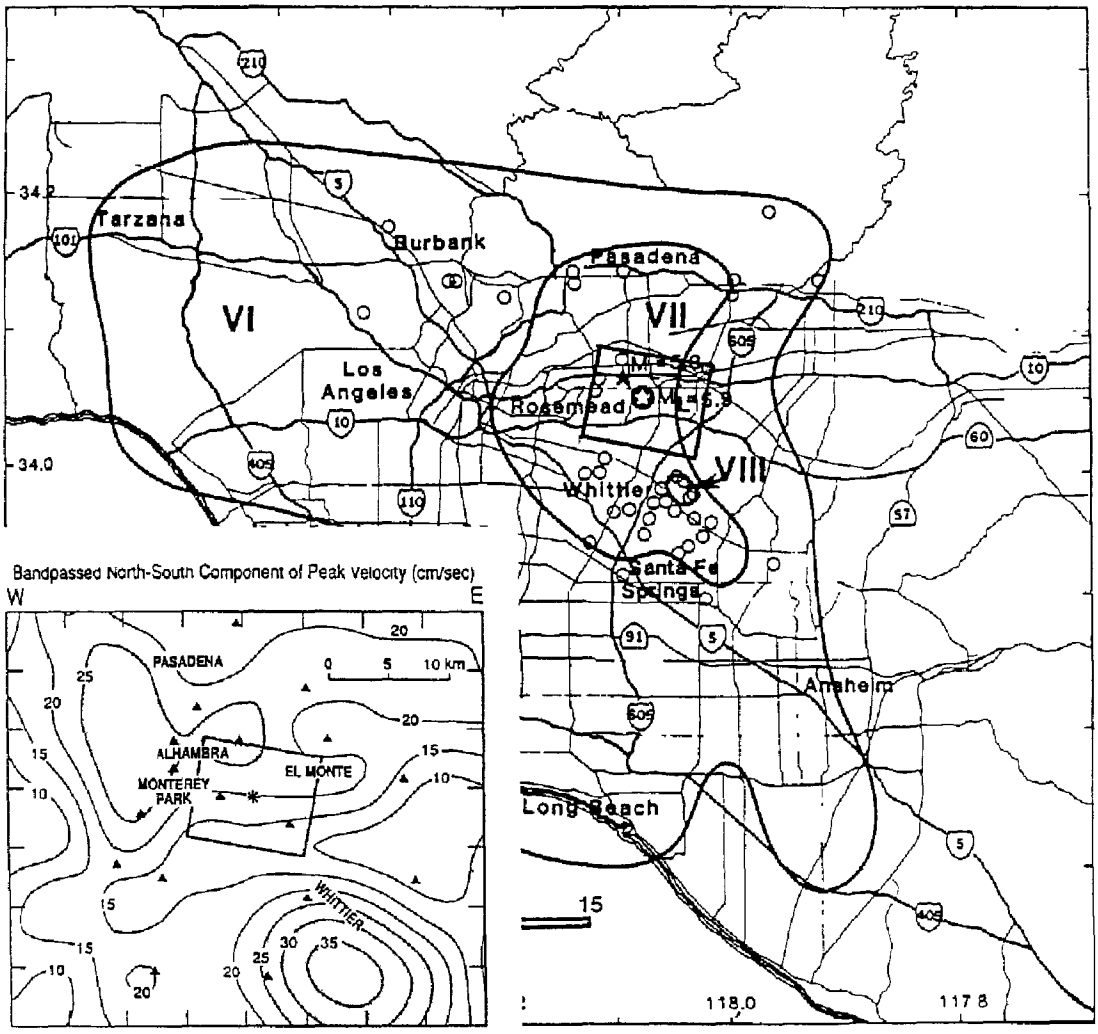

Fig. 1 Regional Modified Mercalli intensity isoseismals of the Los Angeles area in the earthquake of October 1, 1987. The surface projection of the model fault plane is indicated by the rectangular box. Open circles represent the center of the census tracts surveyed. The circled star is the main shock epicenter (after Leyendecker *et al.*). Predicted peak velocities (cm/sec) for the model (b) of Fig. 2 in the bandpass 0.2 to 3.0 Hz are shown on the same scale map at the lower left corner. The stations used are indicated by solid triangles.

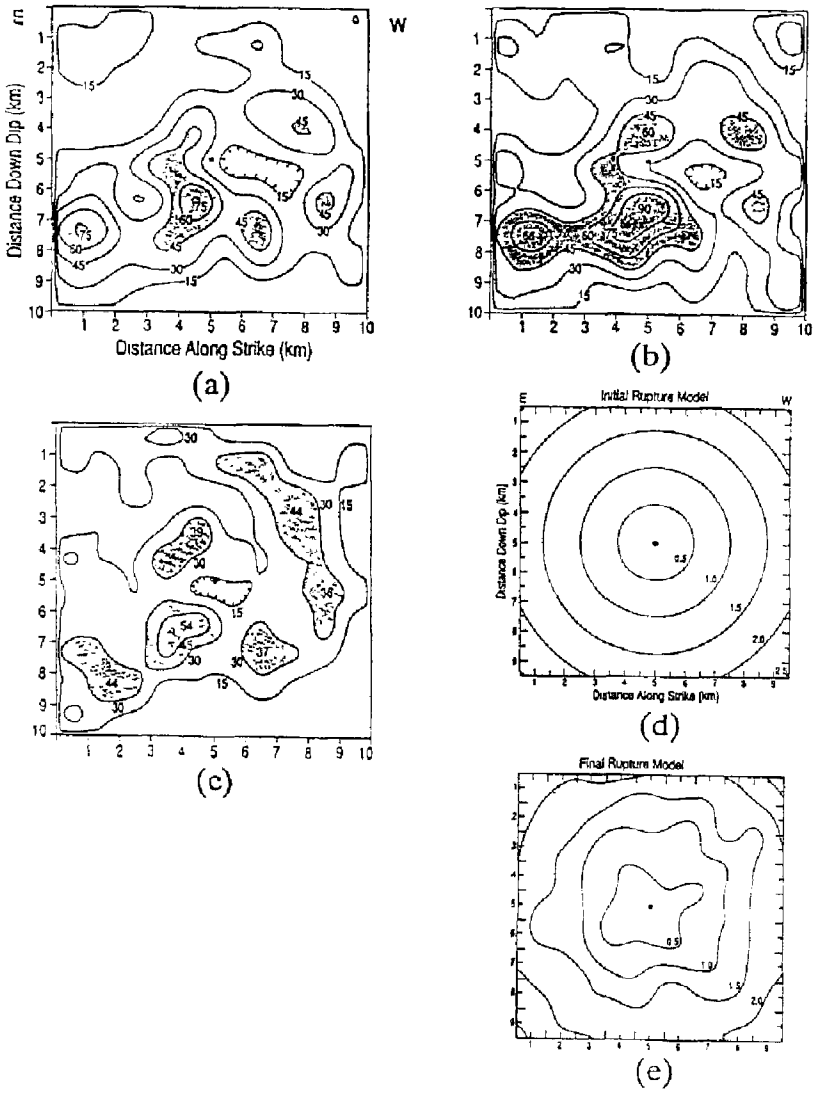

Fig. 2 Contours of slip in centimeters. (a) Each subfault ruptures once. (b) Each subfault is allowed to rupture twice with a certain small time interval in order to allow for a more complex source-time function. In cases of (a) and (b), the rupture progresses with a circular front from the center of the fault at a fixed speed of 2.5 km/s, as shown in (d). (c) Each subfault ruptures once, but the rupture velocity is free to vary. Starting with the initial rupture model of (d), the final rupture model of (e) is obtained.

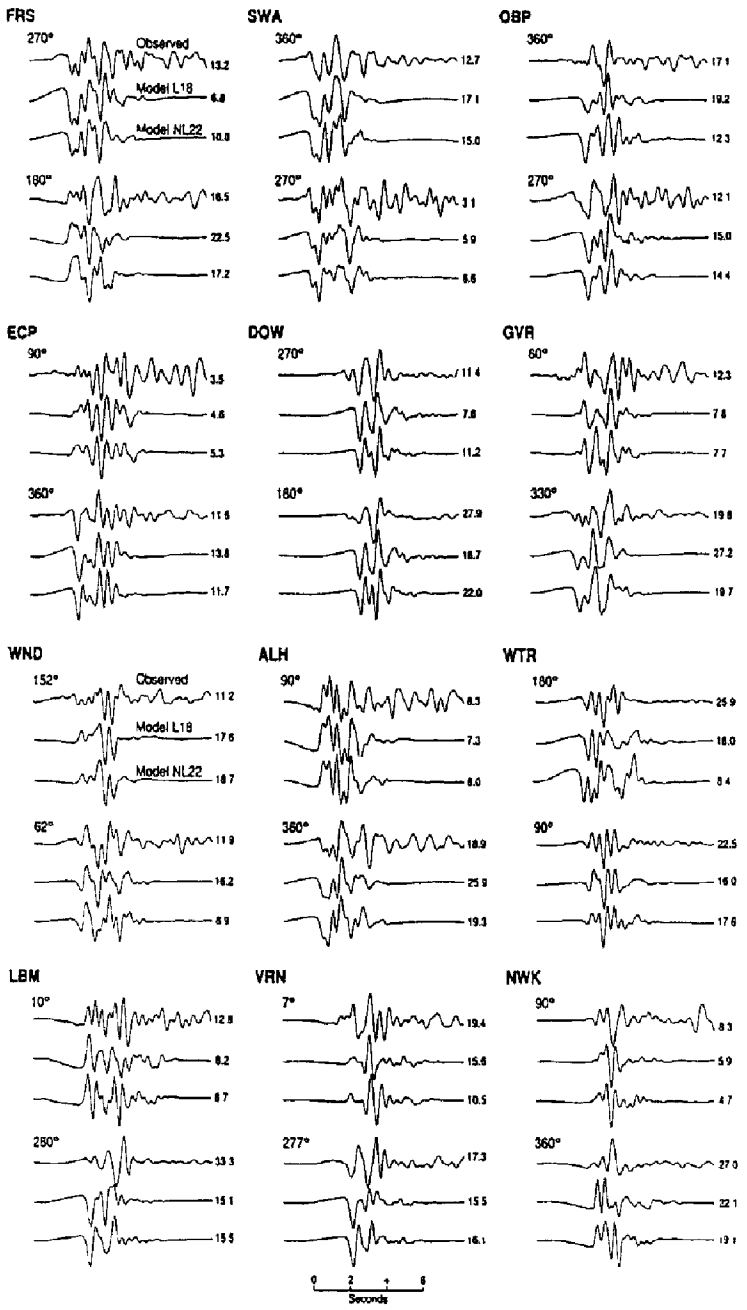

Fig. 3 Comparison of the observed strong-motion velocity records (first trace) with the synthetic ground motion records for the model (b) (second trace) and the model (c) (third trace) of Fig. 2.

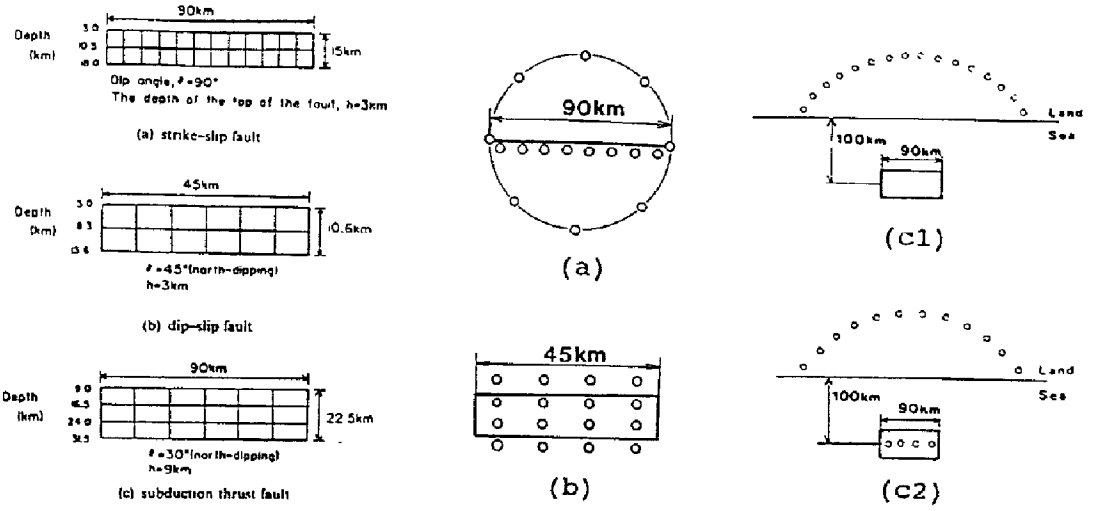

Fig. 4 Fault geometries used for investigating effects of array configurations on the source inversion (side views) and the optimum array configuration obtained for each of 3 fault geometries: (a) strike-slip; (b) dip-slip; and (c) subduction thrust fault (2 cases [c1] without and [c2] with strong-motion ocean bottom seismographs).

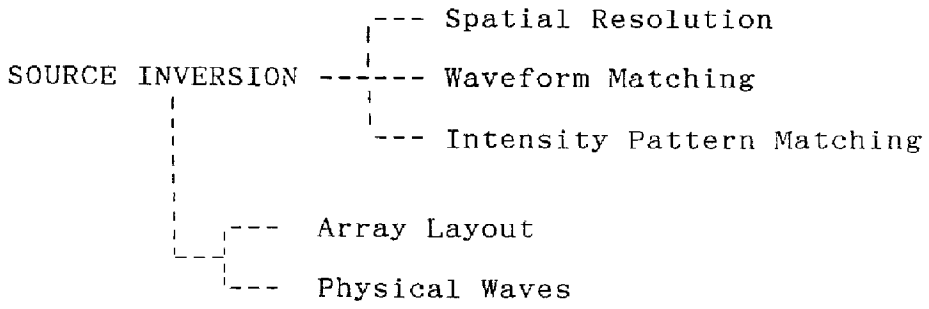

Fig. 5 Schematic display of ideal source inversion in the high-frequency range.

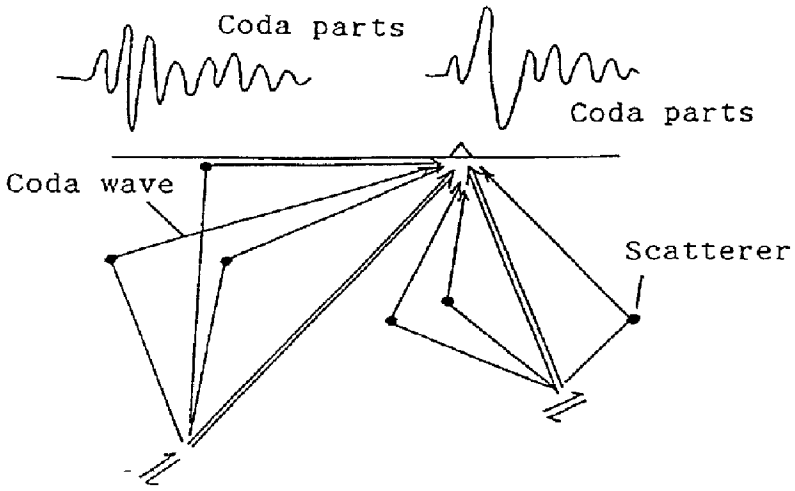

Fig. 6 Schematic explanation of coda parts (later phases after S wave arrivals) of seismograms. Coda parts are composed of scattered waves produced by local heterogeneities.

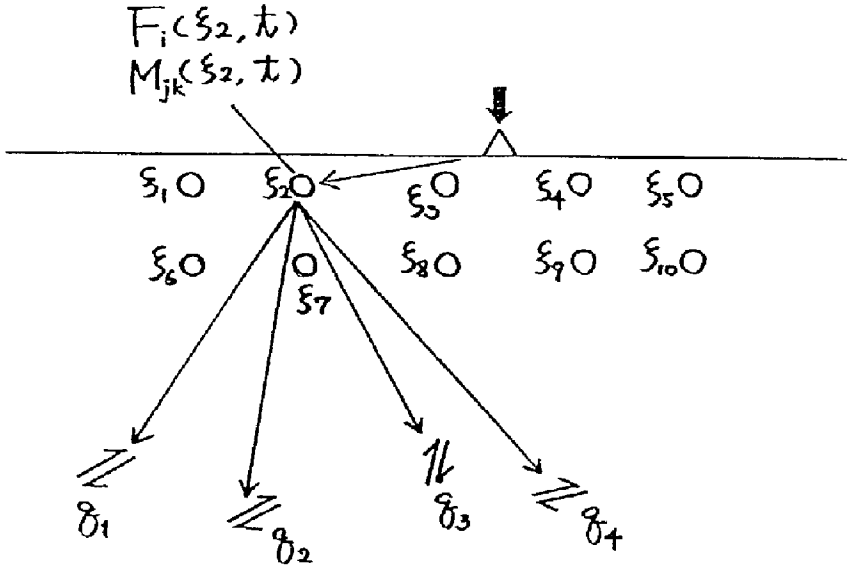

Fig. 7 Schematic display of our idea based upon the reciprocal geometry. We use a set of seismograms from widely distributed local earthquakes observed at a single station. The scattering problem is turned into a radiation problem.

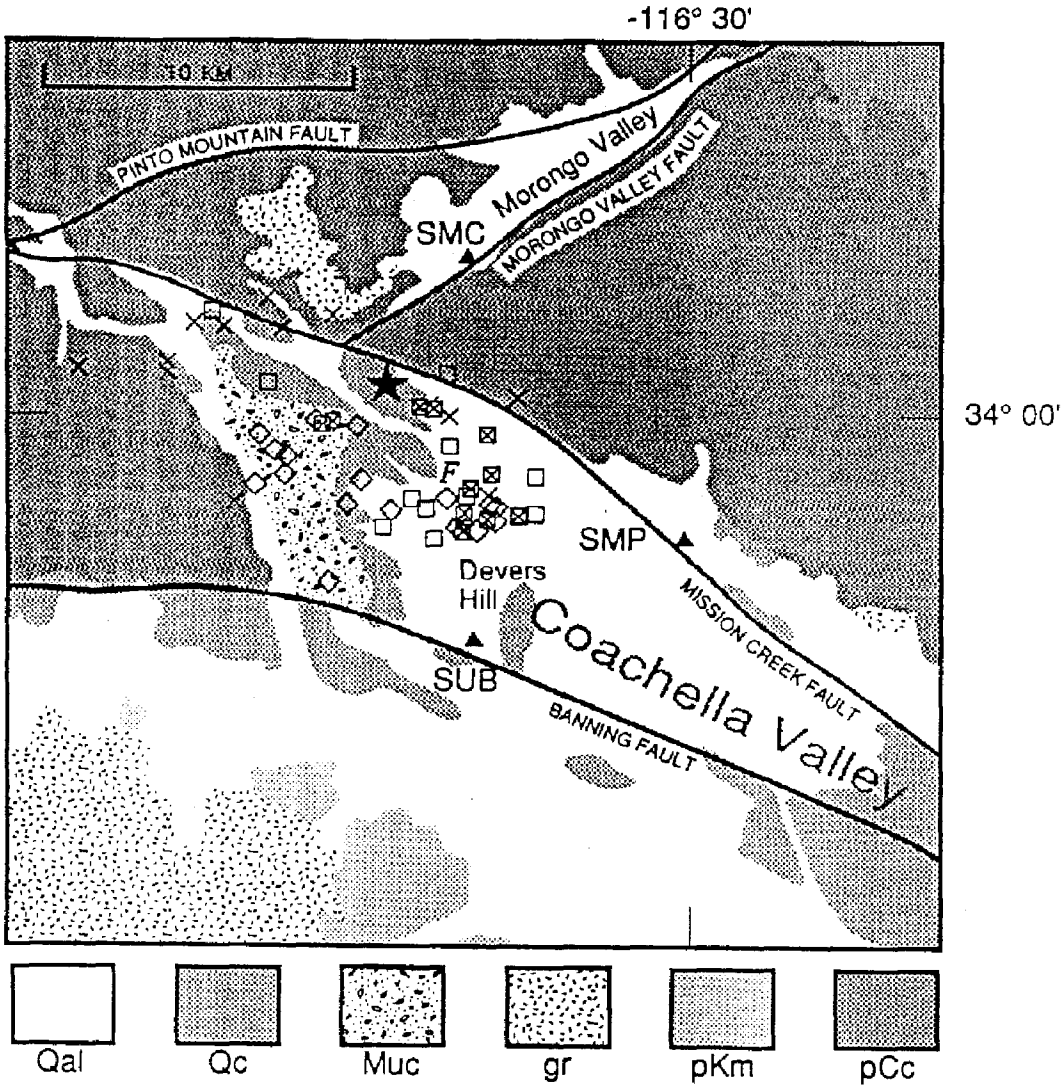

Fig. 8 Simplified geologic map of the North Palm Springs, California, study region, showing the 3 seismic stations, SMC, SMP and SUB. X's, squares and diamonds show the aftershock epicenters recorded by SMC, SMP and SUB, respectively. F, southeast of the main shock epicenter (star), is a locus of strong scattering. The geologic units are (Qal) Quaternary alluvium, (Qc) Pleistocene nonmarine sedimentary deposits, (Muc) upper Miocene nonmarine rocks, (gr) Mesozoic granite, (pKm) pre-Cretaceous metamorphic and metasedimentary complex, and (pPc) Precambrian igneous and metamorphic complex.

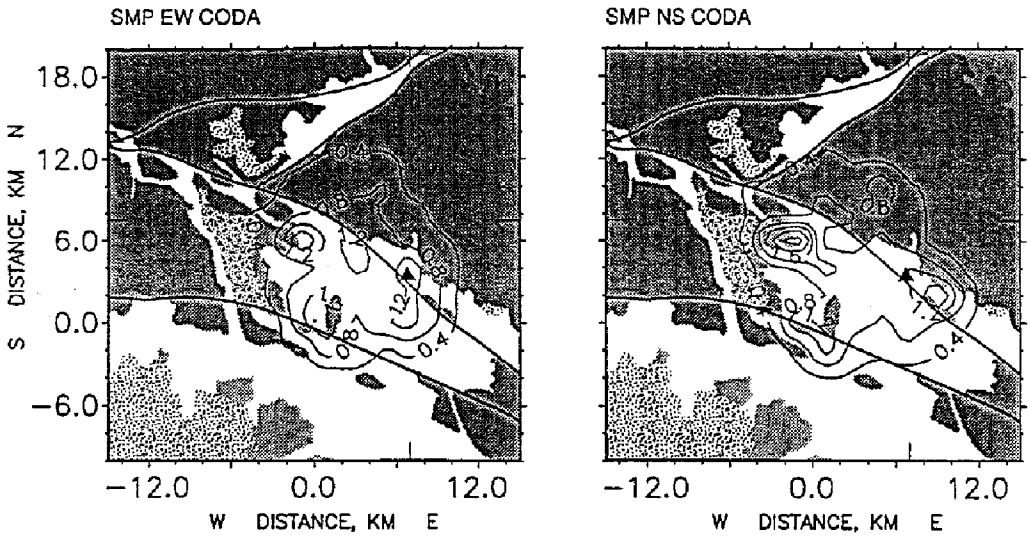

Fig. 9 SMP power distribution (contours) superimposed on the geology of the study area. Seismic data are 13 secs of early coda beginning just after the direct S pulse for the E-W (left) and N-S (right) velocity at SMP (triangle). Scatterer power in both components is peaked at point F [Fig. 8]. Power units are arbitrary.

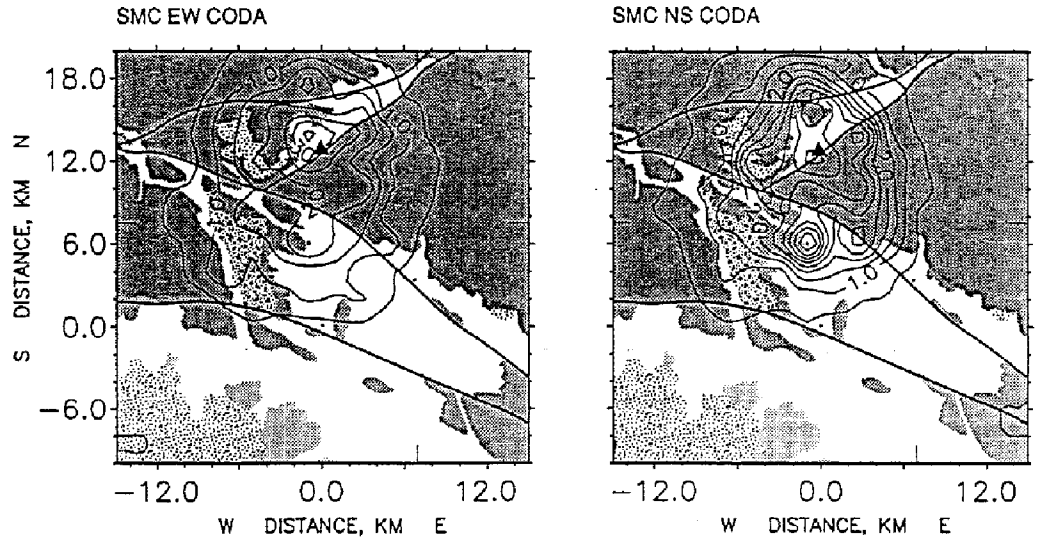

Fig. 10 Power distribution (contours) superimposed on the geology of the study area for SMC (triangle). Power units are arbitrary.

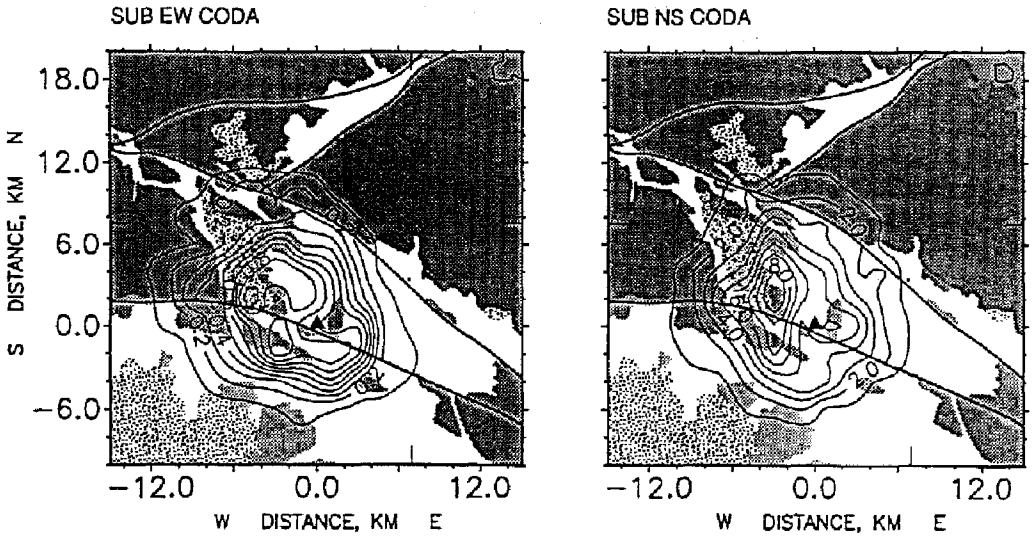

Fig. 11 Power distribution (contours) superimposed on the geology of the study area for SUB (triangle). Unlike SMC and SMP, SUB has no peak at point F [Fig. 8]. Power units are arbitrary.

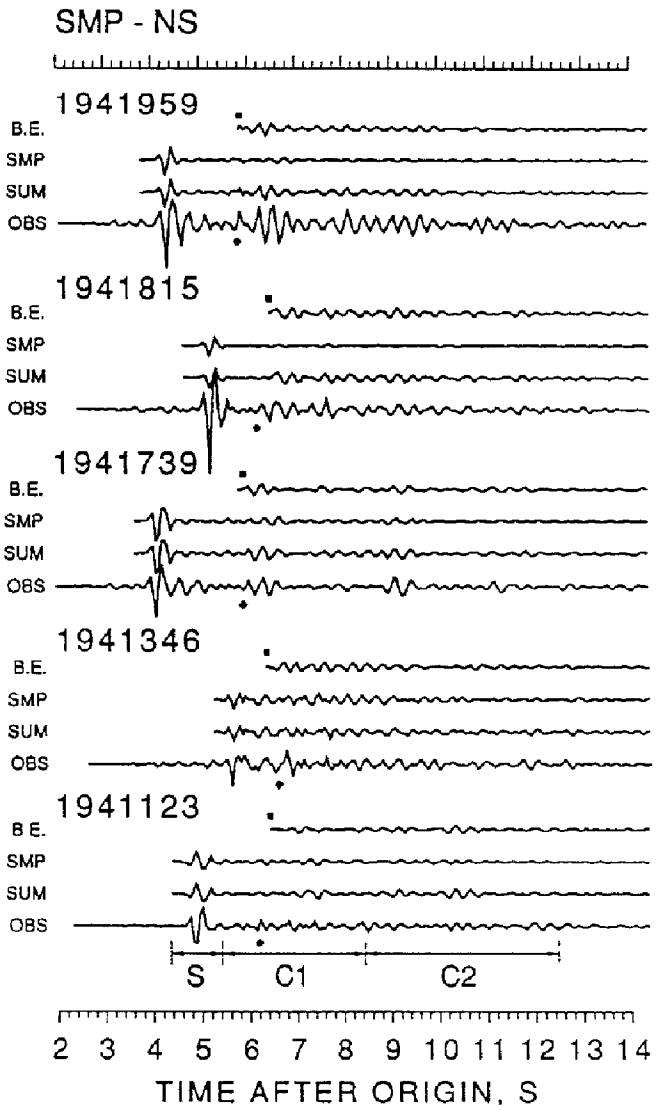

Fig. 12 Observed and predicted N-S ground motions at SMP based on a 2-scatterer model of the region for 5 aftershocks Traces labeled 'B.E.' are the ground motions caused by scattering from point F at the basin edge. 'SMP' indicates motions consisting of direct S and site reverberations modeled by the scatterer at SMP. 'SUM' is the sum of the 'SMP' and 'B.E.' contributions, and 'OBS' is the observed motion Diamonds indicate the onset of a conspicuous phase following S, and squares indicate the arrival time of an S body wave scattered from F.

Lecture 3 SCATTERER INVERSION

Subject 2 The Seismic Coda, Site Effects and Scattering in Alluvial Basins Studied Using Aftershocks of the 1986 North Palm Springs, California, Earthquake as Source Arrays

1. INTRODUCTION

In this paper we examine the complicated ground motions that comprise the early coda immediately following the direct body wave pulses, such as *P* and *S* waves. While the phase and amplitude behavior of direct *P* and *S* pulses can often be modeled deterministically using relatively simple earth structures and propagation methods, the coda is more resistant to such modeling. Consequently, the general goals of this paper are to identify the waves comprising the early coda and to find a semi-deterministic way to model those waves at a seismic station. Our specific application is to the early *S* wave coda of local microearthquakes observed in and around an alluvial basin, but the method we employ may be useful in other frequency bands, epicentral distance ranges, and tectonic settings.

The seismic coda has been studied over many frequency and distance ranges, and several of these previous studies are quite relevant to the work presented here. An important line of research in deterministic interpretation and modeling of *P* coda at teleseismic distances has been carried on by Key (1967), Nikolaev and Troitsky (1987), Lay (1987), Lynnes and Lay (1989), Bannister *et al.* (1990), Gupta *et al.* (1990), and most recently Hedlin *et al.* (1991), who attempted to map near-source and near-receiver scatterer distribution in space based on a deterministic single-scatterer model. The coda of local earthquakes has been very extensively studied, as summarized by Herraiz and Espinoza (1987). A particularly interesting and relevant recent study has been done by Nishigami (1991), who determined a spatial scatterer distribution from local earthquake codas by using a technique similar to those used for teleseismic *P* coda.

It is the connection between the seismic coda and seismic hazard to buildings that has motivated our work. Aki (1988) has written an excellent review of this subject. From an engineering standpoint, one of the most important aspects of the seismic coda is that it increases the duration of strong shaking, causing progressive damage to buildings, as has been observed in Mexico City during the 1985 Michoacan earthquake (Esteva *et al.*, 1989) and in Leninakan during the 1988 Armenian earthquake (Borcherdt *et al* , 1989). The simplest interpretation of the early coda is to regard it as a 'site effect,' i e., some sort of linear transfer function depending only on the receiver location and the geologic structure very near or under the receiver. Two recent alternative characterizations of the site effect are those of Scherbaum (1987), who derives a 1-dimensional velocity structure under the receiver in order to model the site-effect, and Spudich and Miller (1990), who derive empirical site transfer function. However, there is ample evidence that geologic structures far from the receivers can contribute damaging motions in the seismic coda. Hanks (1975) identified strong surface waves in the ground motions of the 1971 San Fernando earthquake, and Liu and Heaton (1984) showed that they were generated at the edges of the Los Angeles and San Fernando basins. Basin-edge surface waves are strongly suspected in the Mexico City and Leninakan examples cited earlier, and have been more recently observed in the Kyoto basin (Horike *et al.*, 1990), the Santa Clara Valley (Frankel *et al.*, 1991), and the Kanto plain (Yamanaka *et al.*, 1989; Phillips *et al.*, 1993). A third mechanism for generation of the early coda has been proposed by Hill and Levander (1984) and Levander and Hill (1985), who showed how the low seismic velocities and extreme geologic heterogeneity near the earth's surface combine to generate ample seismic coda trapped near the surface Spudich and Bostwick (1987) concluded that much of the early seismic coda consisted of energy reverberated in the shallow crust near the seismic station.

Because the simple 'site-effect' model has proved to be inadequate for modeling coda in detail (see, for example, Spudich and Miller, 1990), in this work we try to identify sources of scattered energy, located away from

---

* This lecture note is based on the paper of the same title written by Paul Spudich and Masahiro Iida, submitted to the Bulletin of the Seismological Society of America on July 13, 1993.

the seismic stations, that contribute to the observed coda. We then try to model empirically the waveforms of the scattered energy. We will show that real heterogeneities can be identified from coda waveforms, and that the method we use may be the basis for a scheme for the spatial interpolation of empirical Green's functions. The method we have developed can be used with single-station single-component recordings of ambient microseismicity, and consequently may be applicable to a large volume of seismic data currently in hand.

2. THE 1986 NORTH PALM SPRINGS MAIN SHOCK AND AFTERSHOCKS

The main shock and aftershocks of the North Palm Springs earthquake sequence have been extensively described by Jones *et al* (1986), Hartzell (1989), and Mori and Frankel (1990), and the specific aftershock data set and seismic velocity model we use have previously been displayed and described in detail by Spudich and Miller (1990), so we will dwell only on the aspects that bear upon our work Figure 1 show the epicenters of the main shock and the aftershocks used in this study, along with a generalized geologic map of the region. The main shock and aftershocks probably occurred on the Banning fault, which dips approximately 50° to the NNE. (For the depths of aftershocks, see Spudich and Miller, 1990.) In this region the Mission Creek and Banning faults represent the northern and southern branches of the San Andreas fault. The study area overlaps two alluvial valleys, the Morongo Valley, which is completely contained within the study area, and the northwest end of the Coachella Valley. The valley floors are comprised of low-lying Quaternary units, while the units ringing the valleys have very rugged topography.

An important motivation for our work was the desire to model the main shock ground motion using empirical Green's function summation. The main shock was recorded on several strong-motion accelerographs in the area. GEOS digital event recorders (Borcherdt *et al.*, 1985) were deployed at the strong-motion accelerographs and recorded the specific aftershock data set used in this study. GEOS stations SMC and SMP were cosited with the accelerographs at Morongo Valley Fire Station and Desert Hot Springs, respectively (Figure 1). The aftershock seismograms were recorded on 2-Hz Mark Products L-22 geophones.

Hartzell (1989) derived a rupture model for the main shock by waveform modeling of its ground motions. Hartzell noted that at many stations his synthetic seismograms lacked much of the strong late energy present in the observed motions (see his Figure 12, for example). We believe that the unmodeled late energy consists of S wave coda, and our goal is to identify the geologic heterogeneities that are responsible for producing the coda energy in the aftershock seismograms.

3. METHOD

We use a slightly modified version of the computational method of Spudich and Miller (1990). The general procedure consists of two steps. First, we attempt to identify the geological heterogeneities in the study region which contribute substantial scattered energy to the observed seismic coda. Second, having identified these heterogeneities, we attempt to determine their time-domain contributions to the observed codas. We use the same computer code for both steps, and the analyses are done completely independently for each component of motion at each station. A brief description of the method follows. For additional details, see Spudich and Miller (1990).

Before describing the method, however, we must consider certain notions about scattering in the earth that underlie the method. Our general model is that the top few km of the earth are much more heterogeneous than the deeper part. Not only is the shallow structure complicated, but it is also generally unknown in detail, so that it is impossible to model wave propagation accurately in the shallow crust at high frequencies. The view that the deeper crust is less heterogeneous than the surface is supported by several lines of evidence. First, the earth's surface is a strong velocity discontinuity and scatterer. Key (1967), Bannister *et al.* (1990), Gupta *et al.* (1990) and Hedlin *et al.* (1991) have observed that surface topography is the primary contributor of scattered waves to teleseismic P coda observed at the NORESS array. Using earthquake clusters, Spudich and Bostwick (1987) showed that the early seismic coda of local earthquakes was dominated by near-surface scattering. Hutchings and Wu (1990) observed

that seismograms of a microearthquake recorded at two surface sites 1 km apart are less correlated than seismograms of two microearthquakes separated by 1 km and recorded on a common instrument. These observations reinforce the expectation that the large lateral variations of impedance between surficial units, such as unconsolidated alluvium and granites, are unlikely to persist very deeply owing to pressure and lithification effects. Thus we believe that seismic wavefields in the real earth (at least for the early coda) may resemble those in the lower panel of Figure 14 of Hill and Levander (1984), having complicated behavior near the surface but being simpler at depth. Consequently our method assumes nothing about the Green's functions in the shallow crust, although it assumes that geometric ray theory is generally adequate below a few km depth.

A key concept in Spudich and Miller's (1990) method is that the complicated wave field produced by scattering in a heterogeneous structure can be simulated by complicated artificial sources acting in a simple structure. Consider Figure 2, which shows a schematic seismic experiment in the reciprocal geometry. Owing to Green's function reciprocity, the seismograms from this experiment are identical to those that would be recorded at the surface from a buried microearthquake (Spudich and Bostwick, 1987). An instantaneous point force is applied at the earth's surface and the motions are observed at depth. Suppose that the motions observed at depth are dominated by the direct S wave, site reverberations in the structure very near the point force, and waves scattered from the large impedance contrast at the edge of the basin. Note that although the point force is instantaneous, the waves scattered from the edge of the basin and from the region beneath the force may be quite complicated temporally and prolonged due to multiple scattering, surface waves, etc. In fact, such prolonged scattering from particular surficial heterogeneities can be easily seen in Figure 14 of Hill and Levander (1984), in which the scattered energy appears as sets of concentric wavefronts centered on the heterogeneity. To simulate these scattered waves, we can replace the basin geology by a smooth structure in which ray theory is accurate, and we place force and moment tensor secondary sources having complicated time-functions at the basin edge and beneath the point-force application site. We assume that the waves radiated by these secondary sources propagate as P or S waves to the 'receivers' at depth. This is our conception of the seismic forward problem.

We emphasize that, although our use of force and moment tensor secondary sources is reminiscent of the role of equivalent sources in weak scattering theory (e.g., Aki and Richards, 1980, pp. 732-733), our sources are time-varying and are meant to provide a mechanism to simulate prolonged anisotropic scattering from a complicated geologic structure. They are not intended to be a literal implementation of equivalent sources in weak scattering theory.

In order to find the strongest scatterers in a study region, we postulate a dense grid of trial or hypothetical scatterers (force and moment tensor secondary sources) throughout the volume of interest. This set of assumptions leads to a sparse linear set of equations for the force and moment tensor time series for each hypothetical scatterer (equations 17-25 of Spudich and Miller, 1990). We solve these equations using the iterative scheme of Olson (1987), and we declare the hypothetical scatterers having the strongest equivalent forces and moment tensors to be 'real'.

The iterative procedure has a simple physical interpretation. A single iteration consists of stacking the data seismograms along trajectories that correspond to the travel time curves appropriate for each trial scatterer (Figure 3). If there is a pulse in all the data seismograms that has traveled from the earthquakes to a trial scatterer as a P or S wave, and then from the scatterer to the station by any arbitrary means (e.g., multiple-scattered body wave, higher-mode surface wave), this pulse will be enhanced by the stacking procedure. For example, note in Figure 3 that the travel-times from a particular scatterer to each earthquake completely determine the curves along which data are stacked for that scatterer; the station location is irrelevant, as is the propagation mode between the scatterer and the station. For each scatterer the data are stacked along a set of curves that are progressively time-shifted. Stacking along the t_1 curve for scatterer ξ_i accounts for waves that have traveled from the earthquakes to ξ_i as a direct body wave (S, in our work), and from ξ_i to the station by the fastest possible path. Stacking along the t_2 curve for scatterer ξ_i accounts for waves that have traveled from the earthquakes to ξ_i as a direct S wave, and from ξ_i to the station by a slightly slower path (or as a slightly slower type of wave). By stacking along t_3, t_4, ..., we account for all possible paths, wavetypes, and delays in propagating from the scatterer to the station. The result of the stack over each family of curves is an approximation of the force and moment time series for each trial